# Unraveling Processing-Structure-Electrical Conductivity Relationships of $NaCrO_2$ Cathodes for Na-Ion Batteries

**Mei Luo,[1] Angel L. Ortiz,[2] and Leon L. Shaw [1,z]**

[1] *Department of Mechanical, Materials and Aerospace Engineering, Illinois Institute of Technology, Chicago, Illinois 60616, USA*
[2] *Departamento de Ingeniería Mecánica, Energética y de los Materiales, Universidad de Extremadura, Badajoz 06006, Spain*

The electrical conductivities of $NaCrO_2$ powders synthesized from $Na_2CO_3$ and $Cr_2O_3$ reactants with and without mechanical activation at room temperature before the high temperature reaction are investigated in detail. The effect of holding time at the 900°C reaction on the electrical conductivity is studied as well. It is found that the impurities in the powders and structural defects of the resulting $NaCrO_2$ crystals strongly depend on the synthesis conditions. The impurities and specially the crystal defects, in turn, influence the electrical conductivity of $NaCrO_2$ powders substantially. In particular, the electrical conductivity of $NaCrO_2$ is found to be mainly controlled by the degree of misplacement of $Cr^{+3}$ ions in the Na sites of the O3-$NaCrO_2$ layered structure. The bulk ionic conductivity is determined to be $9.8 \times 10^{-7}$ S/cm when there is only 0.34% misplacement of $Cr^{+3}$ ions in the Na sites, but drops to $1.7 \times 10^{-7}$ S/cm when the misplacement increases to 9.97%. Such a strong correlation of more misplacement with lower electrical conductivity is attributed to blocking of Na ion transport on the Na plane by the misplaced $Cr^{+3}$ ions in the O3-$NaCrO_2$ layered structure.
 [DOI: 10.1149/2.0081915jes]

Manuscript submitted August 15, 2019; revised manuscript received September 29, 2019. Published October 21, 2019.

Sodium-ion batteries (SIBs) have attracted significant attention lately as a strong competitor against Li-ion batteries.[1–14] In this regard, $NaCrO_2$ has emerged as one of the promising cathode materials for use in Na-ion batteries.[1,2,10–14] An important advantage of $NaCrO_2$–based batteries is its high thermal stability, being a safe electrode material because it is more stable than $LiCoO_2$ and $LiFePO_4$.[12] $NaCrO_2$ is isostructural to $LiCrO_2$ (i.e., both have a rhombohedral ($R\bar{3}m$) O3 type layered structure), but it exhibits a different electrochemical behavior. $NaCrO_2$ is able to reversibly deintercalate 0.5 mole of Na ions per formula unit to form $Na_{0.5}CrO_2$, thereby providing a theoretical capacity of 125 mAh/g[2]. However, if deintercalation is conducted beyond 0.5 mole of sodium ions per formula unit the charge capacity reaches ~235 mAh/g, but the discharge capacity is only 90 mAh/g, i.e., irreversible capacity loss occurs.[13] This irreversible capacity loss has been identified to be related to the irreversible migration of Cr ions from the octahedral sites in $CrO_2$ slabs to both tetrahedral and octahedral sites in the interslab layer.[14] Note that structural change also takes place even for deintercalation of 0.5 mole of Na ions per formula unit from $NaCrO_2$ to $Na_{0.5}CrO_2$, leading to the phase transitions of rhombohedral O3 → monoclinic O3 → monoclinic P3 for the charge process.[1] However, the structural change for Na deintercalation within 0.5 mole of Na ions per formula unit is reversible because Cr ions remain at the octahedral sites in $CrO_2$ slabs.[1]

Recently, using in-situ synchrotron X-ray diffractometry, it has been found that mechanical activation through high-energy ball milling at room temperature (RT) can result in significant changes in the synthesis reaction of $NaCrO_2$ powder when compared to reactants without high-energy ball milling.[15] The changes include a decreased onset temperature for the formation of O3-$NaCrO_2$, an increased reaction kinetics, an alternation of the reaction pathway, and a complete reaction at 900°C to form thermally-stable O3-$NaCrO_2$ phase.[15] An earlier study[16] has also revealed that $NaCrO_2$ powders produced with and without mechanical activation at RT before high temperature reaction have different configurations of crystal defects. Furthermore, the electrochemical behaviors of these $NaCrO_2$ crystals are influenced by their structural defects.[16] Specifically, the $NaCrO_2$ crystals resulting from the simple mixture of reactants without high-energy ball milling exhibit gradual decay in the specific capacity over charge/discharge cycles, whereas the $NaCrO_2$ crystals derived from the reactant mixture subjected to high-energy ball milling at RT before the high temperature reaction exhibit high specific capacity with good retention and high coulombic efficiency.[16]

In this study, the electrical conductivities of $NaCrO_2$ powders synthesized with and without mechanical activation at RT before the high temperature reaction are investigated in detail. The effect of holding time at the 900°C reaction on the electrical conductivity is studied as well. With the aid of electrochemical impedance spectroscopy (EIS) it is found that the electrical conductivity of $NaCrO_2$ powder is a strong function of material synthesis conditions. The powder synthesized with mechanical activation at RT before the high temperature reaction and holding at 900°C for 2 h exhibits the highest electrical conductivity among all the $NaCrO_2$ powders investigated here. The trends of electrical conductivity determined from various $NaCrO_2$ powders are interpreted through processing-structural defect-electrical conductivity relationships. To our knowledge, this is the first time that correlations between the structural defect and electrical conductivity of $NaCrO_2$ have been investigated. The detailed findings are described below.

## Methodology

***Material synthesis.—***The starting materials to produce the $NaCrO_2$ cathode materials were $Na_2CO_3$ and $Cr_2O_3$ powders procured from Sigma-Aldrich (St. Louis, MO, USA). $Na_2CO_3$ and $Cr_2O_3$ powders had purities of ≥99.5% and ≥98%, respectively, and they were used as purchased. Based on the scanning electron microscopy (SEM) examination, the particle sizes of these powders were found to be similar, ranging from ~300 to 600 nm. These powders were processed under four different conditions to obtain $NaCrO_2$ powders with different morphological and structural features. Specifically, in the first processing route the $Na_2CO_3$ and $Cr_2O_3$ powders were simply mixed in a 1:1 molar ratio using a mortar and pestle. The hand-grinding time of the $Na_2CO_3$ and $Cr_2O_3$ powder mixture was always controlled to be 5 min after individual $Na_2CO_3$ particles (white powder) being distinguished from $Cr_2O_3$ particles (green powder). The uniformly mixed powder mixture was then pressed into pellets and subjected to a solid-state reaction at 900°C in a tube furnace under a flowing Ar atmosphere either without holding (i.e., cooled down immediately after reaching 900°C) or with 2 h of holding time. The Ar flow rate was controlled as one bubble per second and both the heating and cooling rates were set to be 5°C/min. The resulting powders will be denoted hereafter as "simply mixed and cooled after reaching 900°C" (i.e., SM-cool) and "simply mixed with holding for 2 h at 900°C" (i.e.,

[z] E-mail: lshaw2@iit.edu

SM-2h), respectively. In the second processing route, the equimolar powder mixture of $Na_2CO_3$ and $Cr_2O_3$ was subjected to high-energy ball milling at RT for 10 h under an Ar atmosphere using a shaker mill (8000M, SPEX) with a 10:1 ball-to-powder charge ratio. Stainless steel balls of 6.4 mm in diameter and a stainless container were utilized for high-energy ball milling. Like the simply-mixed powder, the ball-milled powder was also pressed into pellets and subjected to a solid-state reaction at 900°C in Ar with holding times of either 0 h or 2 h. The resulting powders will be denoted hereafter as "ball milled and cooled after reaching 900°C" (i.e., BM-cool) and "ball milled with holding for 2 h at 900°C" (i.e., BM-2h), respectively.

The SM-cool, SM-2h, BM-cool, and BM-2h pellets were grinded into powder using a mortar and pestle for the subsequent characterizations. However, several BM-2h pellets were preserved without grinding into powder in order to compare the electrical conductivities between the pellets without grinding and the powders obtained after grinding. Note that grinding pellets into powder breaks chemical bonds between powder particles and could result in an increase in the interfacial resistance between particles as will be shown later. The samples of BM-2h pellets without grinding is denoted as "BM-2h pellet" hereafter.

***Materials characterizations.***—The size and morphology of the $NaCrO_2$ powder particles were observed using a JEOL JSM 6701-F field emission scanning electron microscopy (FESEM) with an accelerating voltage of 2kV at magnifications of 20,000 X or 50,000 X. To avoid the charging effect, the surface of $NaCrO_2$ particles was coated with silver using a sputter before FESEM imaging.

Structural analysis of the four $NaCrO_2$ powders was conducted by X-ray diffractometry (XRD) using a Bruker D2 diffractometer with a Cu $K\alpha$ source scanning from 10° to 90° with step of 0.02°. Each step takes 1 second, and the 0.19 volt filter is on to filter fluorescence. All samples were mixed with 5 wt% of micrometer-sized Si powder as the internal standard before the data collection, which was introduced to account for the instrumental shifts in the XRD patterns in order to measure lattice parameters precisely. The phases present were first identified with the aid of the PDF2 database, after which the XRD patterns were analyzed using the Rietveld and Pawley methods as described elsewhere.[15,16]

***Characterization of electrical conductivity.***—The electrical conductivity of the four types of $NaCrO_2$ powders was measured using EIS. The measurement procedure used is the one developed previously to measure the ionic conductivity of $Na_3MnCO_3PO_4$ cathode material.[17] Briefly, a special die with a plastic shell and two copper rods (upper and lower punches) was custom made for the EIS measurements. The diameter of the copper rod was 0.96 cm, and the grinded $NaCrO_2$ powders were individually pressed into pellets inside the plastic shell by applying a pressure of 130 MPa to the copper rods. During the EIS measurement, the entire die was clamped with a specially designed vise to ensure a good contact between the pellet and the two copper rods. The EIS measurements were conducted in the frequency range of 100,000 Hz to 100 Hz with an amplitude of 10 mV using a frequency response analyzer (Parstat 4000, Princeton Applied Research). For the sake of comparison, EIS measurements were also performed directly on the as-synthesized BM-2h pellets without grinding into powder, i.e., on the "BM-2h pellet".

## Results and Discussion

***Powder morphological and size features.***—Figure 1 shows representative FESEM images of the four $NaCrO_2$ powders prepared in this study. It can be seen that the SM-cool (Figure 1a) and SM-2h (Figure 1b) powders exhibit some hexagonal particles with flat facets, thus reflecting in principle the crystal structure symmetry of either O3-$NaCrO_2$ ($R\bar{3}m$) or P3-$NaCrO_2$ ($R3m$). The particle sizes of these two types of powders are relatively similar, and range from ~600 nm to 1.2 μm. In contrast, the BM-cool (Figure 1c) and BM-2h (Figure 1d) powders have much smaller particles with sizes ranging from ~80 nm to 500 nm. In addition, the particles in these two powders tend to exhibit round shape with few flat facets. It can thus be inferred that high-energy ball milling at RT for 10 h before the 900°C reaction has refined the particle sizes to the nanoscale, producing smaller particles with much larger specific surface area and round shape. Finally, the fact that BM-2h powder still contains many particles with round shape indicates that 2-h holding at 900°C is not enough for particle growth and changing from round shape to angular shape with flat facets. These differences in powder particle morphology (size and shape) will have an important impact on the electrical conductivity, as will be discussed later.

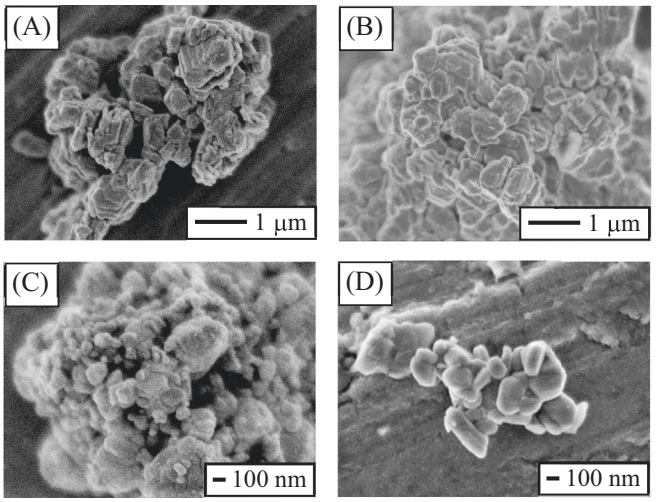


**Figure 1.** FESEM images of (a) SM-cool, (b) SM-2h, (c) BM-cool, and (d) BM-2h powders. Note that different magnifications are used because BM powders are much finer than SM powders.

***Phase composition and structural characteristics.***—Figure 2 shows the XRD patterns collected experimentally for the powder mixtures obtained by blending individually using the mortar and pestle the four $NaCrO_2$ powders synthesized in this study (i.e., the SM-cool, SM-2h, BM-cool, and BM-2h powders) with Si (intentionally added as internal standard), indicating the corresponding phase identification. By way of example, Figure 3 shows one of these four XRD

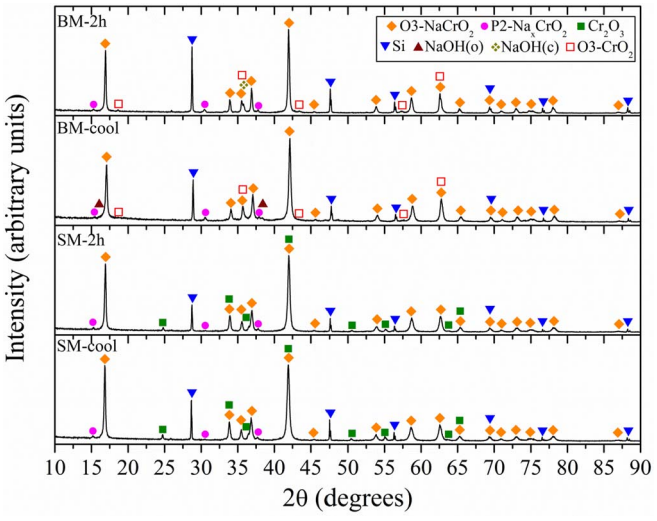


**Figure 2.** XRD patterns of the as-synthesized $NaCrO_2$ powders with and without 2-h holding at 900°C from the mixture of $Na_2CO_3$ and $Cr_2O_3$ reactants with and without mechanical activation at room temperature, as indicated. Peak assignations are included.

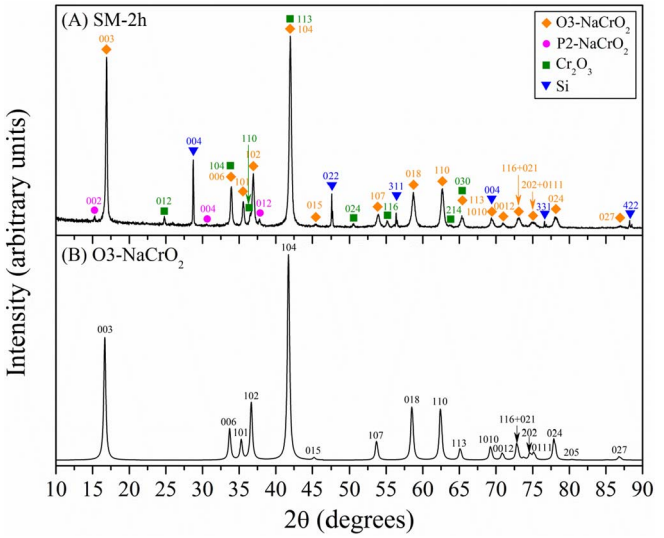


**Figure 3.** XRD patterns: (A) the $NaCrO_2$ powder synthesized with 2-h holding at 900°C from $Na_2CO_3$ and $Cr_2O_3$ reactants without mechanical activation at room temperature, and (B) O3-$NaCrO_2$ without defects in the crystal structure (lattice parameters $a = 2.9747$ Å and $c = 15.9540$ Å). Peak indexing and assignations are included.

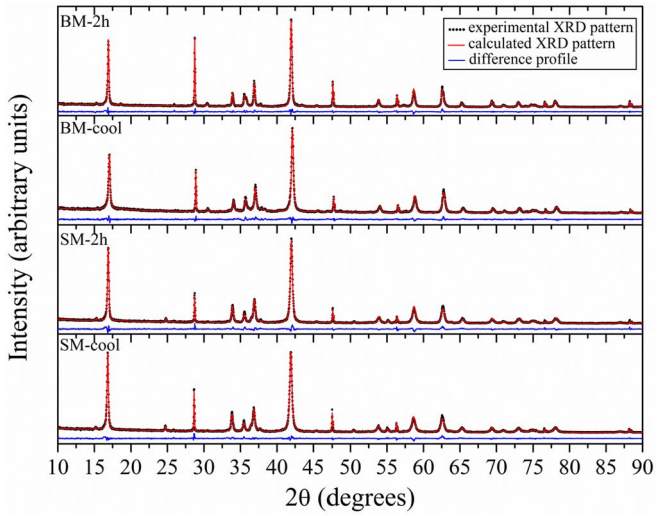


**Figure 4.** Plotted output from the Rietveld refinements of the XRD patterns of the $NaCrO_2$ powders synthesized with and without 2-h holding at 900°C from the mixture of $Na_2CO_3$ and $Cr_2O_3$ reactants with and without mechanical activation at room temperature, as indicated.

patterns with the detailed peak indexing included, together with the standard XRD pattern of O3-$NaCrO_2$ (JCPDS #: 00-025-0819) to be used as reference. The qualitative analysis of the XRD patterns in Figure 2 indicates that all four $NaCrO_2$ powders are predominantly composed of O3-$NaCrO_2$ ($R\bar{3}m$). In addition, the SM-cool and SM-2h powders contain a small amount of P2-$Na_xCrO_2$ ($P6_3/mmc$) and $Cr_2O_3$ ($R\bar{3}c$) phases, while the BM-cool and BM-2h powders also have P2-$Na_xCrO_2$ in minor amount. Additionally, the BM-cool and BM-2h powders contain some NaOH (*Cmcm* in the BM-cool powder and $Fm\bar{3}m$ in the BM-2h powder) and O3-$CrO_2$ ($R\bar{3}m$; more evident for the BM-2h powder).

Although the phase compositions will be quantitatively determined later by Rietveld analyses of the XRD patterns, two interesting conclusions can already be extracted at this stage when the fact is considered that the $Na_2CO_3$ and $Cr_2O_3$ reactants were combined in an equimolar stoichiometric ratio (1:1). First, the $NaCrO_2$ powders produced from the non-mechanically activated reactants are, to a lesser or greater extent, impure because the presence of unreacted $Cr_2O_3$ in both SM-cool and SM-2h powders indicates an incomplete solid-state synthesis reaction at 900°C, attributable to the partial loss of Na source during the high-temperature reaction(s) because there is no unreacted $Na_2O$ in the final powder. On the contrary, the $NaCrO_2$ powders produced from the mechanically activated reactants are intrinsically pure as inferred from the absence of unreacted $Cr_2O_3$ in both BM-cool and BM-2h powders. The presence of a minor P2-$Na_xCrO_2$ phase in BM-cool and BM-2h samples indicates some loss of Na source too, but in a proportion insufficient to prevent the synthesis reaction from being completed. A recent in-situ synchrotron XRD study[15] has demonstrated that this greater powder purity is due to the intensive high-energy ballmilling at RT that speeds up the reaction kinetics substantially and reduces markedly both the onset and completion temperatures for the formation of $NaCrO_2$. Second, the $NaCrO_2$ powders produced from mechanically activated reactants are more hygroscopic than non-mechanically activated counterparts because the presence of some NaOH and O3-$CrO_2$ in both BM-cool and BM-2h powders reflects a slight phase separation of $NaCrO_2$ when in contact with air. According to the in-situ synchrotron XRD study[15] $NaCrO_2$ is stable during the synthesis at 900°C in Ar atmosphere, thus suggesting that NaOH and O3-$CrO_2$ were formed later during the mixing of the $NaCrO_2$ powders with Si and acquisition of XRD patterns in ambient conditions. This greater sensitivity of BM-cool and BM-2h powders to moisture is due to their smaller particle sizes in the nanoscale, as observed in the FESEM images (Figure 1). In any case, this hygroscopy problem will not affect the subsequent electrochemical characterizations because the pellets for EIS measurements were prepared in an argon-filled glove box.

Importantly, detailed comparative analyses reveal that the XRD patterns of SM-cool, SM-2h, BM-cool, and BM-2h powders (Figure 2) differ subtly from the reference XRD pattern of ideal O3-$NaCrO_2$ (Figure 3B). In particular, there are small variations in both the positions and relative intensities of the XRD peaks. These discrepancies between the experimental and theoretical XRD patterns then indicate the existence of crystallographic imperfections in the O3-$NaCrO_2$ crystals of the four powders. More specifically, these crystal imperfections are both distortions of the lattice parameters and existence of lattice point defects. The Rietveld analyses of the XRD patterns will shed more light on this issue.

Figure 4 shows the plotted output from the Rietveld refinements of the XRD patterns of the SM-cool, SM-2h, BM-cool, and BM-2h powders. It can be seen that the Rietveld refinements captured satisfactorily the XRD patterns, with the goodness of the fits ($\chi_r^2$) being lower than 1.3 in all cases. In addition, these Rietveld refinements are very reliable because they are not much worse than the corresponding Pawley refinements, whose plotted outputs are shown in Figure 5.[a] The information extracted from the Rietveld and Pawley analyses are summarized in Table I. Regarding the quantitative phase composition, it can be seen that the Rietveld refinements indicate that SM-cool and SM-2h powders have a 99% purity with 94–95 wt% of O3-$NaCrO_2$ and 4–6 wt% of P2-$Na_xCrO_2$. Within the experimental errors the SM-2h powder would have slightly less P2-$Na_xCrO_2$ but more $Cr_2O_3$ than the SM-cool powder. This is consistent with earlier observations by in-situ synchrotron XRD,[15] which has shown that the O3-$NaCrO_2$ product synthesized without mechanical activation of the reactants has a poor thermal stability. Furthermore, the Rietveld refinements indicate that BM-cool and BM-2h powders are totally pure (100% purity), with 99 wt% of O3-$NaCrO_2$ and ~1 wt% of P2-$Na_xCrO_2$. Note that, in making this statement, it has been considered that the presence of some NaOH in these two powders is an experimental artifact

[a]The Pawley refinement fits the XRD pattern without reference to the crystal structures but simply at angular positions constrained only by the size and symmetry of the unit cell of the crystalline compounds present. The Pawley refinement then gives an indication of the best fit possible from an eventual Rietvled refinement, which fits the XRD pattern bounded to complete crystal structures.

**Table I. Quantitative phase composition and crystallographic information of the O3-$NaCrO_2$ crystals obtained by the Rietveld and Pawley refinements of the XRD patterns. The goodness of each fits is also indicated.**

| | Rietveld refinements | | | | Pawley refinements | |
|---|---|---|---|---|---|---|
| Sample ID | $\chi_r^2$ | Composition (wt%) | Occupancy factors(%) | $NaCrO_2$ lattice parameters (Å) | $\chi_r^2$ | $NaCrO_2$ lattice parameters (Å) |
| SM-cool | 1.20 | O3-$NaCrO_2$ = 93.7<br>P2-$Na_xCrO_2$ = 5.7<br>$Cr_2O_3$ = 0.6 | 3a = $Na^{+1}$ 72.12, $Cr^{+3}$ 9.97, vacancy 17.91<br>3b = $Cr^{+3}$ 98.41, vacancy 1.59<br>6c = $O^{-2}$ 97.86, vacancy 2.14 | $a$ = 2.9763(1)<br>$c$ = 15.984(1) | 1.10 | $a$ = 2.9761(2)<br>$c$ = 15.982(1) |
| SM-2h | 1.30 | O3-$NaCrO_2$ = 95.0<br>P2-$Na_xCrO_2$ = 4.1<br>$Cr_2O_3$ = 0.9 | 3a = $Na^{+1}$ 73.15, $Cr^{+3}$ 9.52, vacancy 17.33<br>3b = $Cr^{+3}$ 98.12, vacancy 1.88<br>6c = $O^{-2}$ 97.22, vacancy 2.78 | $a$ = 2.9751(1)<br>$c$ = 15.9769(9) | 1.18 | $a$ = 2.9750(1)<br>$c$ = 15.978(1) |
| BM-cool | 1.24 | O3-$NaCrO_2$ = 98.98<br>P2-$Na_xCrO_2$ = 1.02 | 3a = $Na^{+1}$ 92.99, $Cr^{+3}$ 0.69, vacancy 6.32<br>3b = $Cr^{+3}$ 100, vacancy 0<br>6c = $O^{-2}$ 97.99, vacancy 2.01 | $a$ = 2.9782(1)<br>$c$ = 15.995(1) | 1.15 | $a$ = 2.9780(3)<br>$c$ = 15.995(2) |
| BM-2h | 1.24 | O3-$NaCrO_2$ = 99.6<br>P2-$Na_xCrO_2$ = 0.4 | 3a = $Na^{+1}$ 93.58, $Cr^{+3}$ 0.34, vacancy 6.08<br>3b = $Cr^{+3}$ 100, vacancy 0<br>6c = $O^{-2}$ 97.86, vacancy 2.14 | $a$ = 2.9787(1)<br>$c$ = 15.9879(9) | 1.22 | $a$ = 2.9784(2)<br>$c$ = 15.986(1) |

derived from their exposure to moisture for XRD characterization. Specifically, it typically took ∼30 min to prepare the XRD samples and 1 hour 15 min for the XRD measurements. This ∼2-h exposure to the air led to the experimental artifact - the presence of NaOH.

The Rietveld refinements also reveal the existence of crystallographic differences in the O3-$NaCrO_2$ crystals of SM-cool, SM-2h, BM-cool, and BM-2h powders. In particular, the unit cells contain different combinations of lattice point defects (vacancies of $Na^{+1}$, $Cr^{+3}$, and $O^{-2}$, as well as misplacement of $Cr^{+3}$ at the $Na^{+1}$ site) and, consequently, have also different dimensions (i.e., lattice parameters). It can be seen in Table I that the O3-$NaCrO_2$ crystals of the four powders have structural defects at the Wyckoff position 3a, which in the ideal crystal structure is fully occupied by $Na^{+1}$. In particular, these defects are both $Na^{+1}$ vacancies and $Cr^{+3}$ misplacement. More importantly, the abundance of these defects is affected by the synthesis conditions, and follows the order SM-cool > SM-2h > BM-cool > BM-2h powders. Note that the configuration of defects at the $Na^{+1}$ layers of the $NaCrO_2$ crystals is particularly relevant because it may play an important role in the electrochemical behavior (sodiation and desodiation) of these cathodes. It can also be seen in Table I that the O3-$NaCrO_2$ crystals of the SM-cool and SM-2h powders have a minor concentration of structural defects at the Wyckoff position 3b, which in the ideal crystal structure is fully occupied by $Cr^{+3}$. These defects are $Cr^{+3}$ vacancies, and its abundance is very similar for the O3-$NaCrO_2$ crystals of both powders. On the contrary, the O3-$NaCrO_2$ crystals of the BM-cool and BM-2h powders have no $Cr^{+3}$ vacancies. Finally, the O3-$NaCrO_2$ crystals of the four powders also have structural defects at the Wyckoff position 6c, which in the ideal crystal structure is fully occupied by $O^{-2}$. These defects in the anion sublattice are $O^{-2}$ vacancies, and are paired with the defects in the cation sublattices to ensure the charge neutrality of the $NaCrO_2$ crystals. Lastly, it is further noted that the vacancies of $Na^{+1}$, $Cr^{+3}$, and $O^{-2}$, and the misplacement of $Cr^{+3}$ at the $Na^{+1}$ site, necessarily induce short-range distortions of the O3-$NaCrO_2$ crystal lattice, which should lead to the overall modification of the lattice parameters. Consistently with this expectation, both the Rietveld and Pawley refinements show that the $NaCrO_2$ crystals in the SM-cool, SM-2h, BM-cool, and BM-2h powders have different lattice parameters due to their different combinations of lattice point defects. In particular, O3-$NaCrO_2$ has lower lattice parameters in the SM-cool and SM-2h powders than in the BM-cool and BM-2h powders, attributable to their higher abundance of lattice point defects (especially at Wyckoff position 3a). This trend is qualitatively consistent with earlier observations by in-situ synchrotron XRD[15] on the SM-2h and BM-2h powders. Note, however, that the lattice parameters measured previously by in-situ synchrotron XRD at 900°C are larger than those measured here by XRD at RT, attributable to the thermal expansion of the unit cell at 900°C.

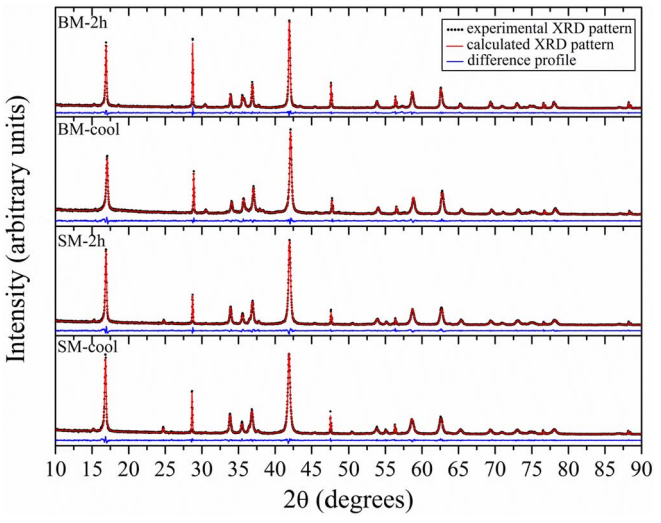


**Figure 5.** Plotted output from the Pawley refinements of the XRD patterns of the $NaCrO_2$ powders synthesized with and without 2-h holding at 900°C from the mixture of $Na_2CO_3$ and $Cr_2O_3$ reactants with and without mechanical activation at room temperature, as indicated.

***Electrical conductivity of powder compacts.***—Figure 6 shows the Nyquist plots measured experimentally for the SM-cool, SM-2h, BM-cool, and BM-2h compacts, together with the modeling results from the equivalent circuit R(QR). It can be seen that the Nyquist plots from these powder compacts exhibit the typical depressed semicircles and that the equivalent circuit R(QR) provides good fitting for all samples with small values of standard errors (< 10%) and $\chi^2$ (< $10^{-3}$). Based on the principles in the impedance measurement of solid electrolyte membranes (such as NASICON),[18–20] the intercept of the depressed semicircle with the X-axis at high frequency has been assigned as the bulk resistance ($R_b$) of $NaCrO_2$ particles and the horizontal length of the semicircle as the sum of the grain boundary resistance ($R_g$) within $NaCrO_2$ particles and the interface resistance ($R_{int}$) between $NaCrO_2$ particles. However, because it is difficult to separate $R_g$ and $R_{int}$, the assumption has been made that the horizontal length of the semicircle is dominated by $R_{int}$. This assumption is supported by the experimental data, as discussed below.

Using the equivalent circuit R(QR), the values of $R_b$ and $R_{int}$ have been determined for all $NaCrO_2$ powder compacts, and with the aid of Eq. 1[17,18,20] the bulk conductivity ($\sigma_b$) and the particle interface

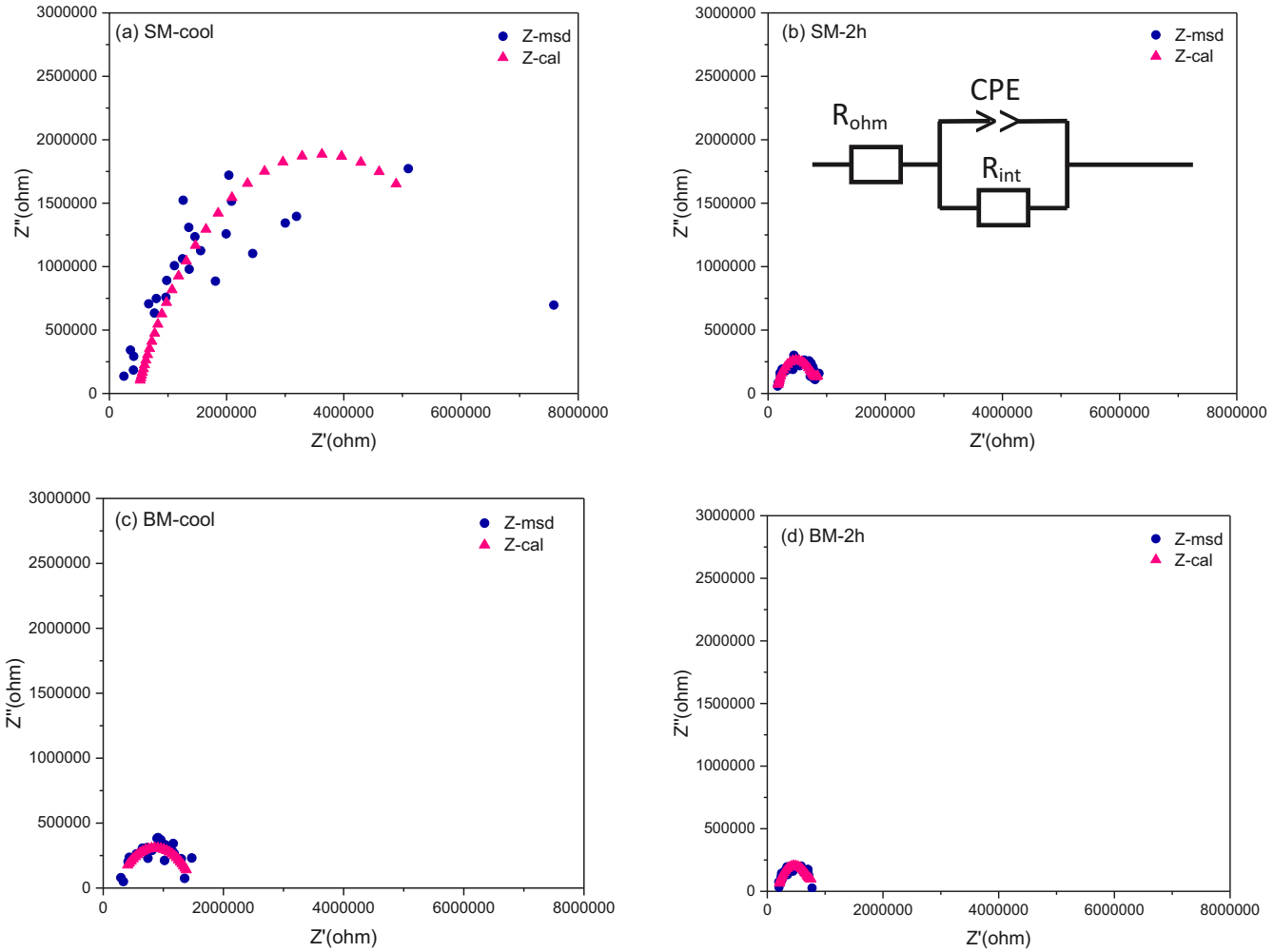


**Figure 6.** EIS curves of (a) SM-cool, (b) SM-2h, (c) BM-cool, and (d) BM-2h $NaCrO_2$ powders. The insert in (b) shows the R(QR) equivalent circuit used in all cases to simulate the EIS data.

conductivity ($\sigma_{int}$) were computed with the inputs of $R_b$ and $R_{int}$, respectively:

$$\sigma = \frac{L}{RA} \quad [1]$$

The physical meaning of $\sigma_b$ is the Na-ion conductivity within crystalline $NaCrO_2$ particles, whereas the physical meaning of $\sigma_{int}$ is the Na-ion conductivity at the interface between $NaCrO_2$ particles. The total conductivity of the $NaCrO_2$ compact ($\sigma_{total}$) is computed using Eq. 1 with the input of the total resistance (i.e., $R_b + R_{int}$). The results are listed in Table II. There are several interesting trends that can be observed from these EIS measurements of the powder compacts, as discussed below.

First, $\sigma_{int}$ is smaller than $\sigma_b$ in all cases. This is understandable because $\sigma_b$ reflects the resistance to Na ion transport inside a particle, whereas $\sigma_{int}$ reflects the resistance to Na ion transport from one particle to another particle across the particle interface. In fact, if the $NaCrO_2$ particles are not in good contact, the resistance to Na ion transport from one particle to another can approach infinite, i.e., $\sigma_{int}$ could become zero while $\sigma_b$ would still be a finite number.

Second, it is noted that "BM-2h pellet" sample has the highest $\sigma_{int}$ among all the samples. This is the case because the EIS data of this sample were collected at the as-synthesized condition without grinding into powder and thus with good chemical bonding and connectivity at the particle interface. In contrast, the EIS data of all other samples were measured after grinding the as-synthesized pellets into fine powder and then pressing the powder into pellets again. As such, the particle interface of all other samples does not have chemical bonding, but with mechanical contact only. Thus, the BM-2h pellet sample has the highest $\sigma_{int}$ among all the samples. It should also be noted that the particle interface conductivities of the powder compacts depend on powder characteristics and the clamping pressure applied to two

**Table II. EIS data of the $NaCrO_2$ powder samples.**

| | $R_b$(ohm) | $\sigma_b$ (S/cm) | $R_{int}$(ohm) | $\sigma_{int}$ (S/cm) | $R_{total}$(ohm) | $\sigma_{total}$ (S/cm) |
|---|---|---|---|---|---|---|
| SM-cool | 4.76E + 05 | 1.75E-07 | 7.83E + 06 | 2.03E-08 | 8.31E + 06 | 1.91E-08 |
| SM-2h | 1.34E + 05 | 5.93E-07 | 6.83E + 05 | 1.17E-07 | 8.17E + 05 | 9.75E-08 |
| BM-cool | 2.47E + 05 | 4.48E-07 | 1.21E + 06 | 1.75E-07 | 1.46E + 06 | 1.45E-07 |
| BM-2h | 1.75E + 05 | 9.82E-07 | 5.96E + 05 | 2.88E-07 | 7.71E + 05 | 2.23E-07 |
| BM-2h pellet | 6.82E + 04 | 8.81E-07 | 7.34E + 04 | 8.17E-07 | 1.42E + 05 | 4.24E-07 |

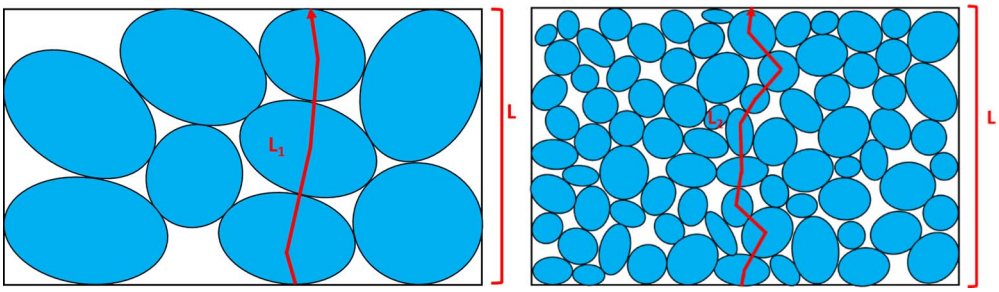


**Figure 7.** Schematic cross-sections of powder compacts with ionic transport length as a function of particle size during EIS measurement. See the text for discussion.

copper rods during the measurement. Higher clamping pressure will result in better mechanical contact between particles, leading to higher $\sigma_{int}$ values. Nevertheless, the clamping pressure was fixed at 130 MPa for all powder samples, and thus the different $\sigma_{int}$ values in this study can be attributed to different powder characteristics.

Third, the following order of decreasing the ionic conductivity for the particle interface conductivity ($\sigma_{int}$) is observed: BM-2h pellet > BM-2h > BM-cool > SM-2h > SM-cool. This order indicates that $NaCrO_2$ with high-energy ball milling before the 900°C reaction have higher $\sigma_{int}$ than $NaCrO_2$ without ball milling. As such, Na ion transport between $NaCrO_2$ particles can be enhanced by mechanical activation before the high temperature reaction. Furthermore, holding at 900°C for 2 h also improves the particle interface conductivity for both BM and SM samples, suggesting that the defect structure or the content of defects on the surface of $NaCrO_2$ particles have changed during 2-h holding at 900°C. It is worthy of pointing out that to the best of our knowledge, this is the first time that the particle interface conductivity has been reported.

Fourth, the order of the bulk ionic conductivity ($\sigma_b$) is slightly different from the particle interface conductivity. Specifically, the bulk ionic conductivity has the order of BM-2h > SM-2h > BM-cool > SM-cool. Although this order is slightly different from $\sigma_{int}$, it still reveals that (*i*) high-energy ball milling before the high temperature reaction enhances the ionic conductivity and (*ii*) holding at 900°C for 2 h improves the ionic conductivity when all other processing conditions are the same. It should be pointed out that the switching from $\sigma_{int}$ (BM-cool) > $\sigma_{int}$ (SM-2h) to $\sigma_b$ (SM-2h) > $\sigma_b$ (BM-cool) should be taken cautiously because it may not be a true phenomenon for the following reasons. First, the bulk conductivities of all samples have been underestimated when Eq. 1 was used to compute the bulk conductivity. This point can be explained with the aid of Figure 7, where powder compacts with different particle sizes are shown schematically. As seen in Eq. 1, the nominal length ($L$) and the nominal cross-sectional area ($A$) of a powder compact are used to convert the resistance ($R$) of the compact to the conductivity ($\sigma$) of the compact. However, actually the true length for electrical conduction is $L_1$ for a powder compact with particle size of $D_1$ (Figure 7a), and $L_1 > L$ because the presence of porosity in the powder compact leads to a tortuous pathway for electrical conduction. Furthermore, the true cross-sectional area $A_1$ is smaller than the nominal one ($A_1 < A$, not shown in Figure 7) because of the porosity in the powder compact. Thus, if $A_1$ and $L_1$ were known, their values should be inserted into Eq. 1 to compute the true bulk conductivity ($\sigma_{b1}$):

$$\sigma_{b1} = \frac{L_1}{R_1 A_1} \quad [2]$$

Since $L_1$ and $A_1$ are unknown, the nominal $L$ and $A$ are used to compute the bulk conductivity of the compact ($\sigma_b$), which is smaller than the true bulk conductivity as shown below:

$$\sigma_{b1} = \frac{L_1}{R_1 A_1} > \sigma_b = \frac{L}{R_1 A} \quad [3]$$

Therefore, the bulk conductivity of a powder compact is underestimated when Eq. 1 with $L$ and $A$ is used to compute the bulk conductivity.

Note however that such an underestimation becomes larger when particle sizes becomes smaller. It is well known that smaller particles result in a lower powder packing density than larger particles when the applied pressure is the same and the particle sizes are in submicrometre or nanometer ranges.[21] Because of the presence of more porosity in the powder compact with small particles of $D_2$ in diameter (Figure 7b), the true length for electrical conduction $L_2$ is larger than $L_1$ in the powder compact with large particles of $D_1$ in diameter. Similar argument leads to the conclusion of $A_2 < A_1$. Therefore, the use of Eq. 1 with $L$ and $A$ results in significant underestimation of the bulk conductivity of a powder compact when particle sizes are very small (Figure 7b). Mathematically, this conclusion can be expressed as:

$$\sigma_{b2} = \frac{L_2}{R_2 A_2} \gg \sigma_b = \frac{L}{R_2 A} \quad [4]$$

Since the particle sizes of SM-2h sample are larger than those of BM-cool sample, the bulk conductivity of SM-2h was therefore underestimated modestly while the bulk conductivity of BM-cool was underestimated significantly when Eq. 1 with $L$ and $A$ was used to compute their respective bulk conductivities. For this reason, the switching from $\sigma_{int}$ (BM-cool) > $\sigma_{int}$ (SM-2h) to $\sigma_b$ (SM-2h) > $\sigma_b$ (BM-cool) should be taken cautiously because it may not be a true phenomenon. In other words, without the significant underestimation of the bulk conductivity of BM-cool sample, it would be likely to have $\sigma_b$ (BM-cool) > $\sigma_b$ (SM-2h), similar to the order of $\sigma_{int}$ (BM-cool) > $\sigma_{int}$ (SM-2h). Whether this is the case is unknown at this stage because the values of $L_1$, $A_1$, $L_2$, and $A_2$ are unknown currently.

Careful consideration of the results in Table II reveals that particle sizes also alter the particle interface conductivity. Thus, it is better to compare ionic conductivities when particle sizes are similar. With this in mind, the following relationships are identified:

$$\sigma_b(\text{BM-2h}) > \sigma_b(\text{BM-cool}) \text{ and } \sigma_{int}(\text{BM-2h}) > \sigma_{int}(\text{BM-cool}) \quad [5]$$

$$\sigma_b(\text{SM-2h}) > \sigma_b(\text{SM-cool}) \text{ and } \sigma_{int}(\text{SM-2h}) > \sigma_{int}(\text{SM-cool}) \quad [6]$$

and also:

$$\sigma_b(\text{BM-2h}) > \sigma_b(\text{SM-2h}) \text{ and } \sigma_{int}(\text{BM-2h}) > \sigma_{int}(\text{SM-2h}) \quad [7]$$

$$\sigma_b(\text{BM-cool}) > \sigma_b(\text{SM-cool}) \text{ and } \sigma_{int}(\text{BM-cool}) > \sigma_{int}(\text{SM-cool}) \quad [8]$$

Eqs. 5 and 6 are valid because comparisons are made with similar particle sizes either in the nanoscale or in the submicrometer range. Eqs. 7 and 8 are also valid because the ionic conductivities of BM samples are significantly underestimated but still larger than those of SM samples. Therefore, it can be concluded that both the bulk ionic conductivity and the conductivity at the particle interface increase with

(*i*) high-energy ball milling before the high temperature reaction and (*ii*) holding at 900°C for 2 h.

Finally, it is noted that $\sigma_b$ (BM-2h) and $\sigma_b$ (BM-2h pellet) are similar but not identical. The similar values of these two bulk conductivities are expected because they both reflect the Na-ion conductivity within crystalline $NaCrO_2$ particles synthesized at the same reaction temperature and holding time. However, their powder packing densities are different with one measured using the as-synthesized pellet (BM-2h pellet sample) and the other measured after grinding the as-synthesized pellet into powder and then pressing the powder into pellets again (BM-2h sample). The BM-2h pellet sample has a denser packing density than the BM-2h sample because the former is in a partially densified state and the latter is a powder compact with the same particle sizes.[21] As such, the length for electrical conduction and the cross-section area for electrical conduction of the BM-2h pellet sample can be regarded to be similar to the nominal values of *L* and *A* in Eq. 1, respectively. In contrast, the length for electrical conduction of the BM-2h sample, *L'*, will be slight longer than *L*, while the cross-section area for electrical conduction of the BM-2h sample, *A'*, will be smaller than *A* because of the looser particle packing of the BM-2h sample (see, for example, Figure 7b). As shown in Eq. 1, the conductivity value depends on the *L'/A'* ratio. Given that *L'* is larger than *L* and *A'* is smaller than *A*, one can expect the *L'/A'* ratio to be deviated from the *L/A* ratio. Therefore, similar values of $\sigma_b$ (BM-2h) and $\sigma_b$ (BM-2h pellet), but not identical, are expected. This is indeed the case because the difference between $\sigma_b$ (BM-2h) and $\sigma_b$ (BM-2h pellet) is only 10% (Table II).

***Processing-structure-electrical conductivity relationships.—***The XRD analysis discussed above has unambiguously revealed that high-energy ball milling at RT before the 900°C reaction has improved the phase purity of the reaction product, i.e., BM-cool and BM-2h powders have 100% $NaCrO_2$, whereas SM-cool and SM-2h powders still contain a small amount of un-reacted $Cr_2O_3$ (Table I). This result is consistent with a previous study[15] showing that high-energy ball milling at RT can increase the reaction driving force to form $NaCrO_2$ as well as enhancing the reaction kinetics, leading to decreases in both the onset and completion temperatures for the formation of $NaCrO_2$. Table I further shows that mechanical activation via high-energy ball milling at RT has led to lower concentrations of P2-$Na_xCrO_2$, a $NaCrO_2$ phase with lower Na contents than O3-$NaCrO_2$, in both BM powders than that in both SM powders. Furthermore, the O3-$NaCrO_2$ phase in BM powders contains higher Na concentrations than SM powders, reflecting more loss of some Na source during high-temperature reactions in SM powders than in BM powders. Interestingly, holding for 2-h at 900°C has similar effects as mechanical activation at RT in promoting the formation of O3-$NaCrO_2$ with higher Na concentrations (although this effect is much smaller than the effect of mechanical activation at RT).

Another very important phenomenon is that misplacement of $Cr^{+3}$ ions in Na sites decreases in the order of BM-2h < BM-cool < SM-2h < SM-cool (Table I), indicating that SM-cool has the largest degree of cation mixing while BM-2h has the smallest cation mixing. Thus, all of the aforementioned results reveal two general trends. First, mechanical activation at RT promotes the formation of the phase pure reaction product with no un-reacted $Cr_2O_3$, leads to O3-$NaCrO_2$ with higher Na concentrations, and minimizes the misplacement of $Cr^{+3}$ ions in Na sites within the O3-$NaCrO_2$ crystal. Second, holding for 2 h at 900°C results in O3-$NaCrO_2$ with slightly higher Na concentrations than without holding at 900°C and minimizes the misplacement of $Cr^{+3}$ ions in Na sites within the O3-$NaCrO_2$ crystal for both SM and BM powders.

Since BM and SM powders have different phase purities and crystal structural defects, one may expect different electrical conductivities from these powders. This is indeed the case, as shown in Figure 6 and Table II. After comparing Tables I and II carefully, several salient trends are noted. First, the lattice parameters of various $NaCrO_2$ crystals in this study do not exhibit a clear trend in affecting the electrical conductivity. Second, the presence of the un-reacted $Cr_2O_3$ is certainly not good, but does not appear to be the key factor affecting the electrical conductivity. This conclusion is supported by the fact that SM-2h powder has a higher concentration of $Cr_2O_3$ than SM-cool powder, but its $\sigma_b$ and $\sigma_{int}$ are both higher than those of SM-cool powder. The reason for this may be related to the small quantity of $Cr_2O_3$ in the powders (< 1.0 wt%). Third, both the degree of misplacement of $Cr^{+3}$ ions in Na sites and the concentration of P2-$Na_xCrO_2$ in powders display a correlation with electrical conductivity, that is, powders with an increased concentration of P2-$Na_xCrO_2$ phase and more misplacement of $Cr^{+3}$ ions in Na sites possess lower electrical conductivity. Although these trends are present, the fact is that the electrical conductivity is mainly controlled by the degree of misplacement of $Cr^{+3}$ ions in Na sites. This conclusion is reached based on the reasoning that the concentration of P2-$Na_xCrO_2$ is small (< 1.1 wt%) in both BM-2h and BM-cool powders, but the former has ~100% higher $\sigma_b$ and ~65% higher $\sigma_{int}$ than the latter. It has been shown above that a small quantity of $Cr_2O_3$ (< 1.0 wt%) will not affect the electrical conductivity of SM powders much. Therefore, it is reasonable to deduce that the electrical conductivity difference between BM-2h and BM-cool powders is not mainly due to the difference in the amount of P2-$Na_xCrO_2$ in the powder because the quantity of P2-$Na_xCrO_2$ in both BM powders is very small (< 1.1 wt%). After ruling out the predominant effect of P2-$Na_xCrO_2$, it can then be concluded that it is the degree of misplacement of $Cr^{+3}$ ions in Na sites that controls electrical conductivity predominantly. Furthermore, the more misplacement (i.e., more cation mixing), the lower the electrical conductivity. Such a correlation indicates that the presence of $Cr^{+3}$ ions on the Na plane has significantly impeded the transport of Na ions on the Na plane in O3-$NaCrO_2$ layered structure. As a result, Na ion conductivity has decreased as the degree of the cation mixing increases.

It is worthy of emphasizing again that the relationships 5, 6, 7 and 8 observed experimentally in this study are due to structural defects (particularly misplacement of $Cr^{+3}$ ions in Na sites), not by the presence of small amounts of P2-$Na_xCrO_2$ and unreacted $Cr_2O_3$ phases. As discussed above, the major effect of P2-$Na_xCrO_2$ on the measured electrical conductivity can be ruled out by comparing the quantities of the P2-phase in BM-2h and BM-cool samples. The quantities of the P2-phase in these two samples are very small (i.e., 0.4% vs. 1.0%, respectively) and similar, but BM-2h has ~100% higher $\sigma_b$ and ~65% higher $\sigma_{int}$ that BM-cool. These results clearly reveal that the P2-phase does not play a critical role in controlling the electrical conductivities of BM-2h and BM-cool samples. The major effect of P2-$Na_xCrO_2$ in controlling the electrical conductivity can also be ruled out by comparing the electrical conductivities of SM-2h and SM-cool samples. As shown in Table I, both SM-2h and SM-cool contain relatively high P2-$Na_xCrO_2$ phase (one being ~5.7% and the other ~4.1%). Thus, the quantities of the P2-phase in these two samples are similar, but the electrical conductivity of SM-2h is about 10 times that of SM-cool. It is unreasonable/unrealistic that ~1.5% difference in the P2-phase has led to one order of magnitude change in the electrical conductivity between SM-2h and SM-cool since both contain relatively high P2-phase quantities. Therefore, the P2-phase does not play a critical role in controlling the measured electrical conductivity in this study. Similar reasoning related to the unreacted $Cr_2O_3$ can also easily rule out the possibility of the major effect of the unreacted $Cr_2O_3$ on the electrical conductivities of SM-2h and SM-cool samples. This discussion has been described in the paragraph above and, therefore, will not be repeated here.

Before closing, it is important to elucidate whether the electrical conductivity measured in this study is mainly ionic conductivity or electronic conductivity. It is proposed that the electrical conductivity measured here is mainly ionic conductivity. This hypothesis is supported by several reasons. First, O3-$NaCrO_2$ has the same crystal structure as $LiCoO_2$ (i.e., both have a rhombohedral ($R\bar{3}m$) O3 type layered structure). It is well known that $Li_xCoO_2$ is an electronic insulator when *x* is close to unity, but becomes a conductor when *x* adopts a lower value (< 1).[22–24] If $NaCrO_2$ behaves similarly as $LiCoO_2$ and the electrical conductivity of $NaCrO_2$ is electronic-conductivity dominated, then $Na_xCrO_2$ ($x < 1$) would have higher electrical

conductivities than $NaCrO_2$. However, this is clearly not the case for the data listed in Tables I and II, which show that SM-cool and SM-2h powders have O3-$Na_xCrO_2$ phase with $x \sim 0.73$ but lower electric conductivities than BM-cool and BM-2h powders (that have O3-$Na_xCrO_2$ phase with $x \sim 0.93$). These results imply that either the electrical conductivity of $NaCrO_2$ is not electronic-conductivity dominated, or $NaCrO_2$ has a very different behavior from $LiCoO_2$ even though they have identical crystal structure. The second reason for the electric conductivity of $NaCrO_2$ being dominated by the ionic conductivity is the good correlation between the degree of misplacement of $Cr^{+3}$ ions in Na sites and the electrical conductivity of $NaCrO_2$. Based on Tables I and II, BM-2h has the lowest degree of misplacement of $Cr^{+3}$ ions in Na sites and the highest electric conductivity, while SM-cool has the highest degree of misplacement of $Cr^{+3}$ ions in Na sites and the lowest electric conductivity. Such correlations strongly suggest that the electrical conductivity of $NaCrO_2$ is dominated by ionic conductivity because high degrees of cation mixing result in blocking and interference of Na ion transport on the Na plane and thus low ionic conductivity.

## Concluding Remarks

This study has unambiguously revealed that the crystal defects and impurities of $NaCrO_2$ product derived from $Na_2CO_3$ and $Cr_2O_3$ reactants depend strongly on the synthesis conditions. The crystal defects and impurities, in turn, influence the electrical conductivity of $NaCrO_2$ powders substantially. The electrical conductivity of $NaCrO_2$ can be altered by about one order of magnitude with the experimental conditions investigated in this study. Specifically, the following detailed conclusions can be made from this study:

1. Mechanical activation via high-energy ball milling at RT promotes the formation of the phase pure reaction product with no un-reacted $Cr_2O_3$, reduces the content of P2-$Na_xCrO_2$ in the final product, results in the formation of O3-$NaCrO_2$ with higher Na concentrations, and minimizes the misplacement of $Cr^{+3}$ ions in Na sites within the O3-$NaCrO_2$ crystals.
2. Holding at 900°C for 2 h promotes the formation of O3-$NaCrO_2$ with slightly higher Na concentrations than without holding at 900°C and minimizes the misplacement of $Cr^{+3}$ ions in Na sites within the O3-$NaCrO_2$ crystals for both SM and BM powders.
3. The combined effects of mechanical activation at RT and holding at 900°C for 2 h lead to the reaction product of $NaCrO_2$ with the following degree of the misplacement of $Cr^{+3}$ ions in Na sites: BM-2h < BM-cool < SM-2h < SM-cool, i.e., SM-cool has the largest degree of cation mixing while BM-2h has the smallest degree of cation mixing.
4. The electrical conductivity of $NaCrO_2$ is mainly controlled by the degree of misplacement of $Cr^{+3}$ ions in Na sites. The more misplacement, the lower the electrical conductivity. Such a correlation is due to blocking of Na ion transport on the Na plane by the misplaced $Cr^{+3}$ ions in O3-$NaCrO_2$ layered structure.
5. The good correlation between the degree of misplacement of $Cr^{+3}$ ions in Na sites and the electrical conductivity of $NaCrO_2$ suggests that the electrical conductivity of $NaCrO_2$ determined through EIS measurement is dominated by the ionic conductivity.

## Acknowledgments

ML and LS are grateful to the financial support from the U.S. National Science Foundation under the award number: DMR–1709959. Fruitful discussion with Prof. Wei Chen is greatly appreciated.

## ORCID

Leon L. Shaw https://orcid.org/0000-0002-2170-1573

## References

1. Y.-N. Zhou, J.-J. Ding, K.-W. Nam, X. Yu, S.-M. Bak, E. Hu et al., *J. Mater. Chem.*, **A 1**, 11130 (2013).
2. S. Komaba, C. Takei, T. Nakayama, A. Ogata, and N. Yabuuchi, *Electrochem. Commun.*, **12**, 355 (2010).
3. M. Sawicki and L. L. Shaw, *RSC Adv.*, **5**, 53129 (2015).
4. V. Palomares, P. Serras, I. Villaluenga, K. B. Hueso, J. Carretero-González, and T. Rojo, *Energy Environ. Sci.*, **5**, 5884 (2012).
5. S.-W. Kim, D.-H. Seo, X. Ma, G. Ceder, and K. Kang, *Advanced Energy Mater.*, **2**, 710 (2012).
6. M. D. Slater, D. Kim, E. Lee, and C. S. Johnson, *Adv. Funct. Mater.*, **23**, 947 (2013).
7. B. L. Ellis and L. F. Nazar, *Curr. Opin. Solid State Mater. Sci.*, **16**, 168 (2012).
8. H. Pan, Y.-S. Hu, and L. Chen, *Energy Environ. Sci.*, **6**, 2338 (2013).
9. S. P. Ong, V. L. Chevrier, G. Hautier, A. Jain, C. Moore, S. Kim et al., *Energy Environ. Sci.*, **4**, 3680 (2011).
10. C. Y. Chen, K. Matsumoto, T. Nohira, R. Hagiwara, A. Fukunaga, S. Sakai, K. Nitta, and S. Inazawa, *J. Power Sources*, **237**, 52 (2013).
11. J. J. Ding, Y.-N. Zhou, Q. Sun, and Z.-W. Fu, *Electrochem. Commun.*, **22**, 85 (2012).
12. X. Xia and J. R. Dahn, *Electrochem. Solid-State Lett.*, **15**, A1 (2012).
13. S. Komaba, T. Nakayama, A. Ogata, T. Shimizu, C. Takei, S. Takada, A. Hokura, and I. Nakai, *ECS Trans.*, **16**, 43 (2009).
14. K. Kubota, I. Ikeuchi, T. Nakayama, C. Takei, N. Yabuuchi, H. Shiiba, M. Nakayama, and S. Komaba, *J. Phys. Chem.*, **119**, 166 (2015).
15. M. Luo, A. L. Ortiz, F. Guo, Z. Shi, L. Li, Y. Ren, X. Zhang, Z. Chen, L. Shaw, and W. Chen, *Materialia*, **5**, 100172 (2019).
16. M. Sawicki, A. L. Ortiz, M. Luo, and L. L. Shaw, *ChemElectroChem.*, **4**, 3222 (2017).
17. C. Wang, M. Sawicki, J. Kaduk, and L. Shaw, *J. Electrochem. Soc.*, **162**, A1601 (2015).
18. A. G. Jolley, G. Cohn, G. T. Hitz, and E. D. Wachsman, *Ionics.*, **21**, 3031 (2015).
19. W. Luo, Y. Gong, Y. Zhu et al., *J. Am. Chem. Soc.*, **138**, 12258 (2016).
20. R. O. Fuentes, F. M. Figueiredo, F. M. B. Marques, and J. I. Franco, **140**, 173 (2001).
21. R. M. German and Powder Metallurgy Science, *Metal Powder Industries Federation* (1984).
22. M. Shibuya, T. Nishina, T. Matsue, and I. Ichida, *J. Electrochem. Soc.*, **146**, 3157 (1996).
23. M. D. Levi, G. Salitra, B. Markovsky, H. Teller D. Aurbach, U. Heider, and L. Heider, *J. Electrochem. Soc.*, **146**, 1279 (1999).
24. F. Nobili, F. Croce, B. Scrosati, and R. Marassi, *Chem. Mater.*, **13**, 1642 (2001).